A Comparison of Separated and Combined Winding Concepts for Bearingless Centrifugal Pumps

Klaus Raggl[†], Thomas Nussbaumer[**] and Johann W. Kolar[*]

[†*]Power Electronic Systems Laboratory, ETH Zurich, Zurich, Switzerland
[**] Levitronix GmbH Zurich, Switzerland

ABSTRACT

Bearingless centrifugal pump systems are employed in the semiconductor, pharmaceutical and medical industries due to their facility for pumping high purity fluids without particle contamination. Two types of forces have to be generated by the stator units, namely bearing forces for achieving magnetic levitation, and drive forces for producing the needed pump torque. The generation of these forces requires bearing and drive windings, which can be realized as separate bearing and drive coils or as identical, combined coils on the stator claws. In this paper, a detailed comparison between these two winding concepts is undertaken, whereby the copper losses, the power electronics losses, and the achievable pump output pressure are evaluated for both concepts. For each criterion a ratio of improvement is calculated analytically which allows evaluation of the performance of the two winding concepts for any given pump operating point and design. Finally, also practical features such as control complexity, cabling effort and manufacturability are discussed and measurements on prototype systems are carried out to validate the considerations.

Keywords: Bearingless motor, Winding concepts, Permanent magnet synchronous machine, Magnetic levitation

1. Introduction

Bearingless motors have been extensively investigated recently and successfully employed in high purity environments such as the semiconductor, pharmaceutical and medical industries. The reasons can be found in their great variety of benefits such as the non-contact bearing capability and therefore, the lack of mechanical wearing, lubricants and seals [1-3].

However, new applications and arising demands require a further optimization of the pump systems regarding the maximum achievable hydraulic pump pressure and reduction of the pump volume, the power losses and the costs of the pump system [4],[5]. One approach to achieve a cost reduction is the omittance of displacement sensors by applying sensorless control techniques [6]-[9]. Another crucial element in the optimization of the pump system is the motor part. Here, the required bearing and drive forces can be generated for the same motor setup by different winding concepts of the stator coils. As will be shown in this paper, this may have a large influence on the copper and electronics losses and the pump performance.

The comparison which has already been published in parts in [10] is based on a centrifugal pump system with a
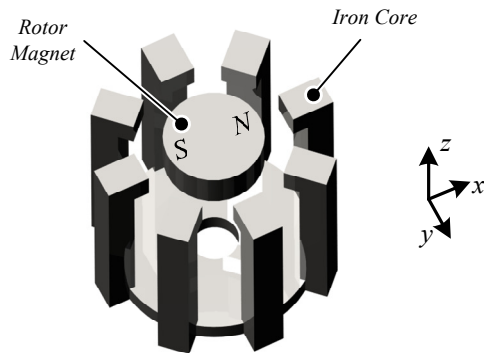

Fig. 1 Basic setup of a bearingless slice motor for a centrifugal pump with a diametrically magnetized rotor

diametrically magnetized, one pole pair rotor (cf. Fig. 1). The stator consists of eight claws which carry the drive and/or bearing coils. The optimum pole pair number for the drive system (p_d = 1) and the bearing system (p_b = 2) for this setup have been discussed extensively in literature [11]-[14] and the motor setup as shown in Fig. 1 is defined for the comparison in this paper.

Fig. 2 shows the two considered winding concepts that will be analyzed in the following (only two of the eight stator claws are shown exemplarily for sake of better illustration). For the conventional setup (cf. Fig. 2(a)) separate coils are used to impress the bearing and the drive forces independently as it is done in various designs, for example for a permanent magnet [11],[15-18], reluctance [19] and induction motors [20]-[21]. Thus, the design of the drive and bearing unit can be carried out separately. Additionally, for this concept various windings can be connected in series to compose a phase or can also be wound over various stator claws (as is the case here for the drive winding, cf. Fig. 2(a)).

An alternative way is to generate the needed bearing and drive forces in each coil by combined windings (cf. Fig. 2(b)) as it is also done in polyphase bearingless motor configurations [22-28]. Here, on each stator claw only a single coil is placed, which carries jointly the required drive and bearing ampere-turns. The question arises now, which winding concept is preferable in terms of losses and

performance. This issue has not been analyzed in detail in literature until now and is therefore addressed here in this paper.
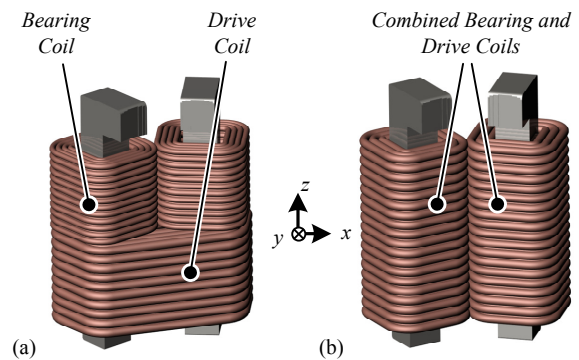

Fig. 2 Winding concepts for the bearingless pump-separated coils (a) and combined coils (b) (detailed view on two of the eight stator claws)

The subsequent discussion of these two winding concepts is based on the following assumptions:

- Same motor setup (iron circuit, rotor magnet size and magnetization)
- Same required bearing force and torque for both concepts
- Same maximum allowable current density
- Same winding factor

After a short explication of the bearing and drive force generation in section 2, the detailed comparison is performed in the subsequent sections, i.e.:

- Section 3: Copper losses
- Section 4: Power electronics losses
- Section 5: Maximum achievable pump pressure / rotation speed

Finally, experimental measurements on existing pump systems with separated and combined coils verify the correctness of the considerations and results in section 6.

2. Force generation

In this section, the generation of the bearing and drive forces is explained for the two winding concepts based on the motor setup at hand (cf. Fig. 1). The fundamentals are essential for the understanding of the comparison in the subsequent sections.
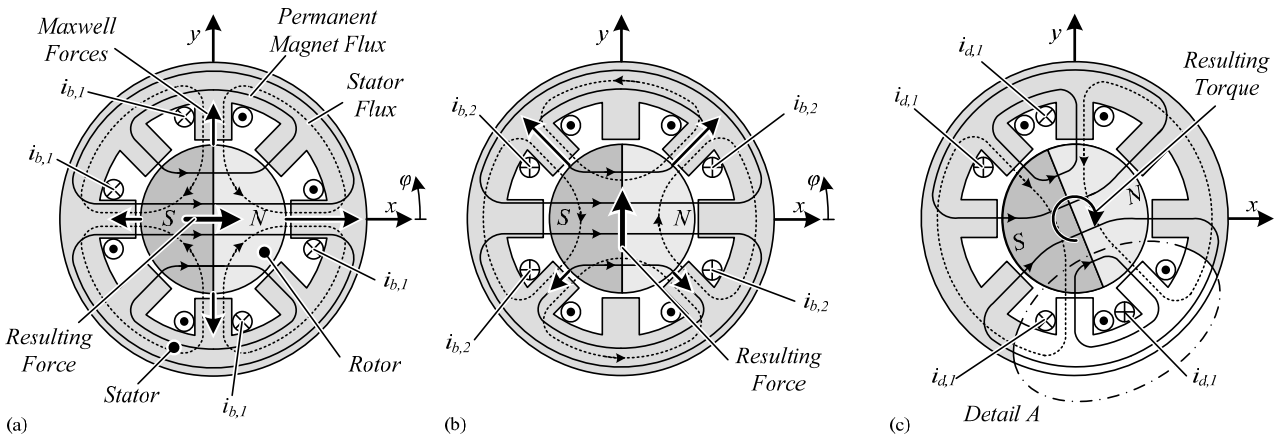
Fig. 3   (a) Maxwell Force generation in magnet direction   (b) Maxwell Force generation perpendicular to magnet direction
(c) Torque generation with one phase – the second phase is rotated by 90° The solid flux lines are originated from the PM, while the dotted lines indicate the flux due to the stator currents

The principle of the bearing force generation is shown in Fig. 3(a) for resulting forces in magnetic direction (in this case in x-direction) and in Fig. 3(b) for resulting forces perpendicular to the magnet direction (y-direction). For the sake of better illustration, a top view on an equivalent 2-dimensional motor setup with radial claws is shown in Fig. 3(a) to 4 instead of the 3-dimensional setup as depicted in Fig. 1. Furthermore, only radial Maxwell forces between the claws and the rotor are shown in these figures. As has been shown in [29], tangential Maxwell forces, which are also acting on the rotor, sum up to a total force which is always pointing in the same direction as the radial forces in this setup. The magnetized rotor introduces a magnetic field into the stator (solid lines schematically depicted in Fig. 3(a)) directed from the magnetic north pole through the stator to the magnetic south pole. By applying a current $i_{b,1}$ in four of the eight coils, as shown in Fig. 3(a), a superposed magnetic field (dashed lines) is generated. This field, impressed by the coils, leads to an attenuation of the permanent magnetic field in the left air gap and a reinforcement of the magnet field in the right air gap. According to the Maxwell equations these two magnetic fields cause radial forces F on the magnetic surface directed to the stator, where its value is proportional to the square of the air gap field density B: $F \sim B^2$. With the shown magnet and current direction of $i_{b,1}$ in Fig. 3(a) a resulting force in positive x-direction is built

up.

Fig. 3(b) shows the bearing force generation perpendicular to the magnetic direction. In this case, the permanent magnetic field and the stator field are superposed again. With a current $i_{b,2}$ flowing through the remaining coils in the directions shown in Fig. 3(b) a resulting force in positive y-direction is built up. From this result, it is possible to generate forces in x- and y-direction for any angular rotor position.

The torque generation by one drive phase is depicted in Fig. 3(c). The impressed drive current $i_{d,1}$ in the shown coils leads to a magnetic field orthographically to the magnetic rotor field for this specific angular rotor position. This leads to a resulting torque on the rotor as shown in Fig. 3(c). By applying sinusoidal currents in drive phase *1* ($i_{d,1}$) and drive phase *2* ($i_{d,2}$) with $i_{d,2}$ having a phase shift of 90° with respect to $i_{d,1}$ and being placed on the four remaining stator claws in an analogous manner, a constant torque can be generated.

2.1 Separated Coils

Since the same currents (e.g. $i_{b,1}$ in Fig. 3(a) and $i_{b,2}$ in Fig. 3(b), respectively) are flowing through the shown coils, they can be directly connected in series. Therefore, only two bearing phases are needed to ensure levitation in x- and y-direction. Another specialty of this winding configuration is the appearing induced voltages in the
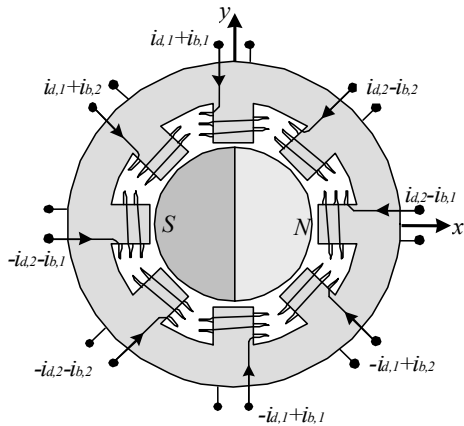
Fig. 4   Needed currents in each coil in case of combined coils

bearing coils are eliminated due to the symmetry. This leads to a higher available coil voltage and hence to increased bearing dynamics.

The drive coils shown in Fig. 3(c) can be connected in series too, such that in total four phases have to be energized in order to generate autonomous forces in *x*- and *y*-direction and a torque in *z*-direction for this coil setup. Since two neighbored drive coils always carry the same current, the drive windings can be wound over two claws, as shown in Fig. 2(a). As shown in [10] this slightly reduces the average winding length and therefore the copper losses of the separated coils.
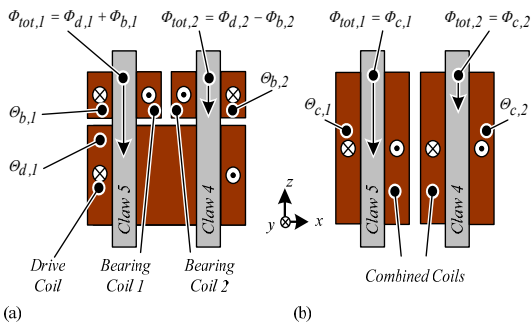
2.2 Combined Coils

Fig. 5   Separated (a) and combined (b) winding concepts for a bearingless slice motor with eight claws. For better visibility only two of the eight stator claws are shown

Out of Figure 3 the needed currents per coil and claw can be ascertained for the setup with combined windings on each claw. The resulting situation is shown in Fig. 4. One can see easily that in the case of combined coils a simplification by connecting two or more coils in series is not possible anymore due to different currents needed in each coil, such that eight phases have to be energized in this case.

3. Copper Losses

For the explanation of the copper loss comparison two neighboring (of the eight) stator claws are exemplarily considered (e.g. claws *4* and *5* in Fig. 4). The situation at the other claws can be analyzed in an analogous way by symmetry considerations. In Fig. 5 the magnetic flux generation in these neighbored claws through the bearing and drive ampere-turns is illustrated for the case of separated (cf. Fig. 5(a)) and combined (cf. Fig. 5(b)) coils, with the ampere-turns $\Theta_{b,1}$ and $\Theta_{b,2}$ needed to impress the bearing flux, the drive $\Theta_{d,1}$ and the combined ampere-turns ($\Theta_{c,1}$ and $\Theta_{c,2}$), each defined by $\Theta_i = i_i \cdot N_i$ with the respective phase currents i_i and the winding numbers N_i

Due to the winding arrangement of the separated coils, the flux phase difference between two neighbored bearing coils (cf. Fig. 6) has to be 90° to ensure levitation [2]. As a matter of fact, the needed ampere-turns in the bearing have the same frequency as the drive ampere-turns in the case of a centrifugal pump, where a steady asymmetric force is acting on the rotor directed to the hydraulic outlet of the pump due to a pressure loss at the hydraulic pump outlet (adjusted in φ-direction, cf. Fig. 3(a) and 3(b)), which causes a load angle φ between the drive and bearing ampere-turns (cf. Fig 6). The needed ampere-turns for separated coils are generally given by

$$
\begin{bmatrix}
\Theta_{b,1} \\
\Theta_{b,2} \\
\Theta_{d,1} \\
\Theta_{d,2}
\end{bmatrix}
=
\begin{bmatrix}
\hat{\Theta}_b \cdot \sin(\omega t - \varphi) \\
\hat{\Theta}_b \cdot \cos(\omega t - \varphi) \\
\hat{\Theta}_d \cdot \sin(\omega t) \\
\hat{\Theta}_d \cdot \cos(\omega t)
\end{bmatrix}.
\tag{1}
$$

Exemplarily, a typical operation state at $\omega t = \omega t_1$ will be examined in the following (cf. Fig. 6). Here, the

impressed magnetic flux of the bearing coil 2 is operating against the impressed flux of the drive coil in the iron claw 4 on the right hand side (cf. Fig. 5(a)). Therefore, the resulting magnetic flux $\Phi_{tot,2}$ in that claw is reduced due to the counteraction of the individual magnetic fluxes. Obviously, in the case of combined coils (Fig. 5(b)) the same resulting flux $\Phi_{tot,2}$ in claw 4 on the right hand side can be built up by less ampere-turns, whereas lower copper losses occur in this setup for the same impressed magnetic flux $\Phi_{tot,2}$. This loss reduction will be quantified in the following.
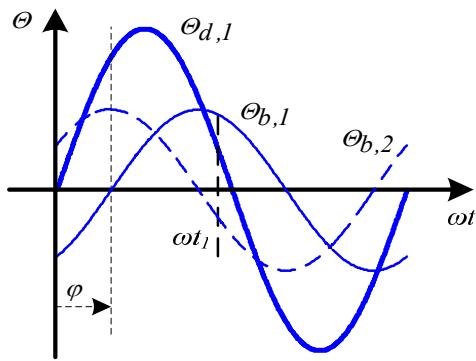

Fig 6　General curves of ampere-turns in bearing and drive with a global force acting on the rotor

Generally, the appearing copper losses per coil can be written as

$$P_{cu}(\Theta_i) = R_i \cdot \left(\frac{\Theta_{rms,i}}{N_i} \right)^2 \tag{2}$$

in dependency on the phase resistance $R_i = N_i^2 \cdot \frac{\rho_{cu} \cdot l_{m,i}}{A_i \cdot k_f}$ with the copper resistivity ρ_{cu}, the average winding length $l_{m,i}$ of one winding, the winding factor k_f and the total coil cross sectional area A_i of the bearing, drive or combined windings of one claw. Here, $\Theta_{rms,i}$ stands for the *rms* value of the ampere-turns Θ_i per coil given in (1). The scaling of R_i with N_i^2 arises from the fact that the total coil cross sectional area A_i is set constant which causes the effective copper area of each winding to decrease for an increasing number of turns N_i. With this, the copper losses can be written as

$$P_{cu,i}(\Theta) = \frac{\rho_{cu} \cdot l_{m,i}}{A_i \cdot k_f} \cdot \Theta_{rms,i}^2. \tag{3}$$

As a result, the copper losses for each claw and coil can be calculated with the needed ampere-turns for separated coils given in (1) inserted in (3). The total copper losses for all drive and bearing coils are finally given by

$$P_{cu,s} = 4 \cdot P_{cu}(\Theta_{b,1}) + 4 \cdot P_{cu}(\Theta_{b,2}) + 4 \cdot P_{cu}(\Theta_{d,1}) + 4 \cdot P_{cu}(\Theta_{d,2}). \tag{4}$$

In (4) the same average winding length l_m for drive and bearing coils has been assumed, i.e. the drive windings are wound around the stator claws individually in order to simplify the calculations in the first instant. By winding the drive coils around two stator claws (cf. Fig. 2) the average winding length can be slightly reduced by a geometric dependent factor k_{lm} as defined in (15) in [10]. For the sake of simplicity, this loss reduction will not be considered in the following examinations.

In the case of combined coils, on the other hand, the needed ampere-turns $\Theta_{c,i}$ per claw can be written as a combination of the needed bearing $\Theta_{b,i}$ and drive $\Theta_{d,i}$ ampere-turns to (cf. Fig. 4)

$$\begin{bmatrix} \Theta_{c,1} \\ \Theta_{c,2} \\ \Theta_{c,3} \\ \Theta_{c,4} \\ \Theta_{c,5} \\ \Theta_{c,6} \\ \Theta_{c,7} \\ \Theta_{c,8} \end{bmatrix} = \begin{bmatrix} \Theta_{b,1} - \Theta_{d,1} \\ \Theta_{b,2} - \Theta_{d,1} \\ -\Theta_{b,1} + \Theta_{d,2} \\ -\Theta_{b,2} + \Theta_{d,2} \\ \Theta_{b,1} + \Theta_{d,1} \\ \Theta_{b,2} + \Theta_{d,1} \\ -\Theta_{b,1} - \Theta_{d,2} \\ -\Theta_{b,2} - \Theta_{d,2} \end{bmatrix}. \tag{5}$$

The resulting copper losses for combined coils are given by the sum of the individual coil losses

$$P_{cu,c} = \sum_{i=1}^{8} P_{cu}(\Theta_{c,i}). \tag{6}$$

With (4) and (6) the copper loss reduction by implementing combined coils is given by

$$\frac{P_{cu,c}}{P_{cu,s}} = \frac{\hat{\Theta}_b^2 + \hat{\Theta}_d^2}{\left(\hat{\Theta}_b + \hat{\Theta}_d\right)^2} \tag{7}$$

in dependency on the needed ampere-turns for bearing and drive. It has to be stated that (7) is only valid under the assumption of the same current density for the separated bearing and drive coils

$$J_{s,rms} = \frac{\Theta_{b,rms}}{A_b} = \frac{\Theta_{d,rms}}{A_d} \tag{8}$$

and the assumption that the total coil volumes (i.e. total cross sectional areas) are the same for both setups:

$$A_c = A_d + A_b . \tag{9}$$

With these assumptions it becomes clear, that the loss reduction for the combined coils is achieved through a lower resulting current density $J_{c,rms} < J_{s,rms}$ in some coils. This fact can also be utilized for a volume reduction instead of a copper loss reduction which leads to a general trade-off situation between minimal volume and minimal losses [10].

The calculated copper loss ratio is shown in Fig. 7 with dependency on the ampere-turns ratio Θ_d / Θ_b with the previously mentioned winding factor k_{lm}. For a drive winding configuration as shown in Fig. 2(a), where the drive coil is wound over two claws, k_{lm} is typically in the range of 0.9 [10].
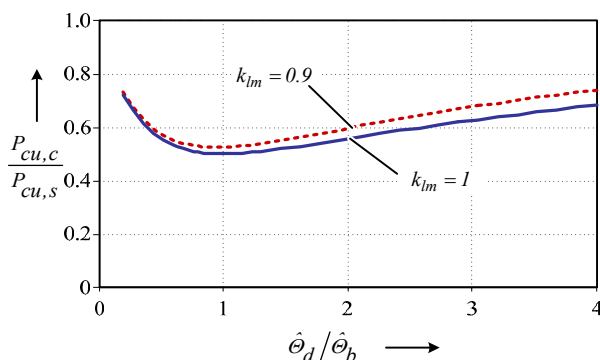

Fig. 7 Copper loss ratio $P_{cu,c} / P_{cu,s}$ over ampere-turn ratio in dependency on the winding length factor k_{lm}

One can see that there is a maximum loss reduction of about 50% (for $k_{lm} = 1$) at an ampere-turns ratio of $\Theta_d / \Theta_b = 1$. This ampere-turns ratio Θ_d / Θ_b is dependent on the pump operating point and is typically in the range of 2-3 for high pressure pumps. In this range a copper loss reduction of about 40% is possible. A realistic value of improvement will be in the range of 30%- 40% due to the fact that non-sinusoidal, non-repetitive forces will always be present in the system to a certain extent (e.g. due to noise in the sensor signals) and the previously mentioned loss reduction for separated coils by the winding factor k_{lm}.

An interesting result is the independence of the copper loss reduction of the load angle φ. While the individual losses of the claws show a dependency on φ, this dependency disappears by summation of the losses of all coils. In Fig. 8 the copper loss reduction of the combined coil setup with respect to the separated coil setup for each of the eight claws is shown for different operation points. A change in the load angle φ from 0° to 22.5° with an ampere-turns ratio $\Theta_d / \Theta_b = 1$ is depicted in Fig. 8(a) and Fig. 8(b). The influence of an ampere-turns ratio change from 1 to 4 can be seen by comparing Fig. 8(a) and Fig. 8(c).

4. Power Electronics Losses

The losses occurring in the power electronics are a further important issue for the comparison of the two concepts. Here, first two power electronics inverter setups have to be found, which allow a fair comparison. Subsequently, the currents, which are required for delivering the same power to the pump in both winding configurations, have to be calculated in order to evaluate the power electronics losses. It is important to choose an optimal number of turns for each configuration in order to perform a fair comparison. In the course of deriving the equations, some simplifications will be made in order to limit the mathematical effort and keep the focus on the essentials.

In case of separated coils, two drive phases and two bearing phases have to be driven by the power electronics inverter stage, each consisting of four coils connected in series (from the viewpoint of the required current to generate the torque, drive windings with N turns over two
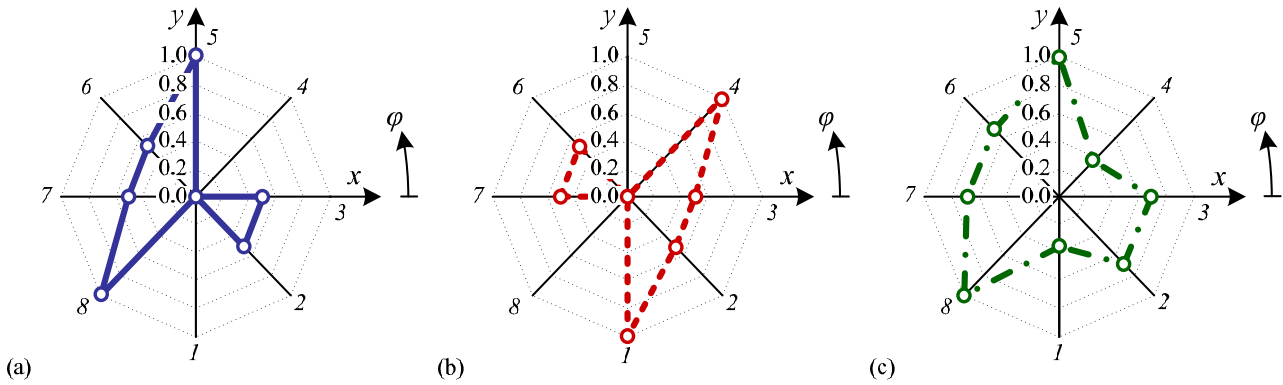
Fig. 8 Copper loss ratio $P_{cu,c}$ / $P_{cu,s}$ for each claw: (a) Θ_d / $\Theta_b = 1$, $\varphi = 0°$; (b) Θ_d / $\Theta_b = 1$, $\varphi = 22.5°$; (c) Θ_d / $\Theta_b = 4$, $\varphi = 0°$;
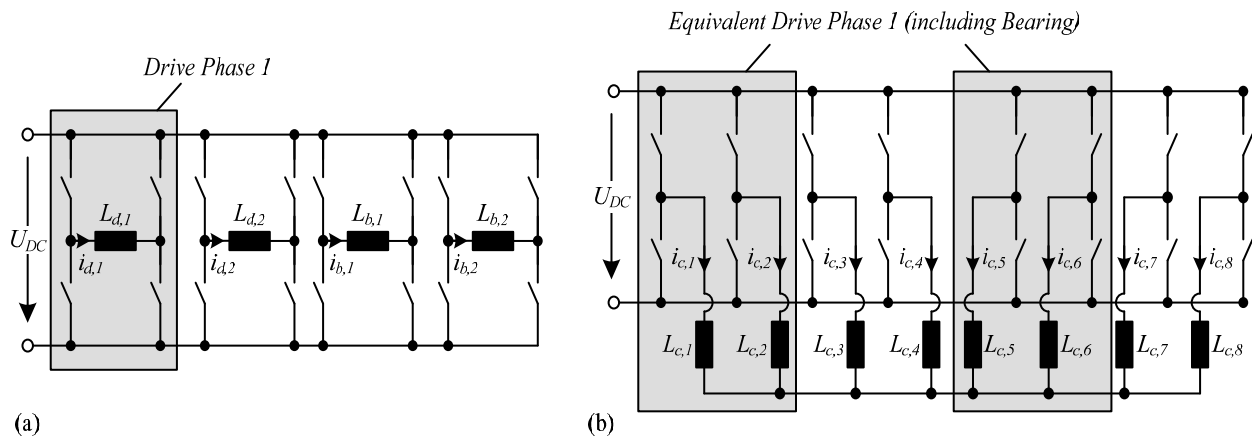

Fig. 9 Power electronics topologies for equal output power for separated (a) and combined (b) coils

coils are equivalent with a serial connection of two coils with each N turns as mentioned already in section 2). In contrast, eight coils have to be energized individually in the case of combined coils. Thus, a full-bridge setup is chosen for the separated coils (cf. Fig. 9(a)) and a half-bridge setup with star-connected coils is considered for the combined coils (cf. Fig. 9(b)). With this, both setups consist of the same amount of semiconductors featuring the same current ratings and are supplied by the same DC-link voltage.

4.1 Separated Coils

Looking at only one drive phase (cf. Fig. 9(a)) in case

of separated coils, an equivalent circuit diagram consisting of four drive coils connected in series (cf. Fig 3(c)) can be drawn, which is shown in Fig. 10(a). Each coil is characterized[1] by a coil inductance L_s and an induced voltage $\hat{U}_{ind,s} = k_u·N_s·n$ caused by the electromotive force (EMF). Here, the index s again indicates the separated coil setup. Due to the series connection of the four drive coils, the total inductance is $4·L_s$ and the induced voltage $4·\hat{U}_{ind,s}$ is appearing in the drive phase.

For typical pump applications, a constant flow rate is required. With this, the required mechanical power is

---

[1] The winding resistance is omitted here for sake of simplicity.

scaling with

$$P_{req} = k_P \cdot n^2 \tag{10}$$

with the pump constant k_P and the rotation speed n in rpm.
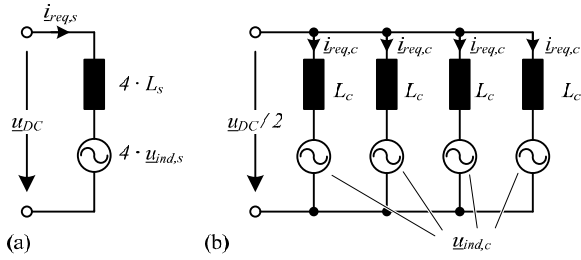

(a)   (b)

Fig. 10 Equivalent circuit diagrams for separated (a) and combined (b) coils of one drive phase needed for the calculation of the required phase current $\hat{I}_{req}$.

With the mechanical power delivered by one drive phase according to

$$P_{mech,s} = \frac{1}{2}\left(4 \cdot \hat{U}_{ind,s} \cdot \hat{I}_{req,s}\right) \tag{11}$$

the required phase current $\hat{I}_{req,s}$ can be calculated for the separated coils by equalizing P_{req} and $P_{mech,s}$ to

$$\hat{I}_{req,s} = \frac{k_P n}{2 k_u N_s}. \tag{12}$$

However, the maximum feasible current amplitude is limited by the voltage across the coil in combination with its inductance

$$\hat{I}_{feas} = \frac{60 \cdot \sqrt{U_{DC}^2 - \hat{U}_{ind}^2}}{2 \pi n L}. \tag{13}$$

In case of separated coils (13) can be written as

$$\hat{I}_{feas,s} = \frac{60 \cdot \sqrt{U_{DC}^2 - 16 \cdot k_u^2 \cdot n^2 \cdot N_s^2}}{2 \pi n k_L N_s^2 \, 4}, \tag{14}$$

since the coil inductance scales according to $L_s = k_L \cdot N_s^2$ with a constant inductance factor k_L.

Looking at (12) and Fig. 11 one can see that the required current is decreasing with an increasing number of turns N. Hence, an infinite number of windings would lead to a minimum required current. However, since the maximum feasible current $\hat{I}_{feas}$ is decreasing quadratically with growing N (cf. (14) and Fig. 11) the optimum
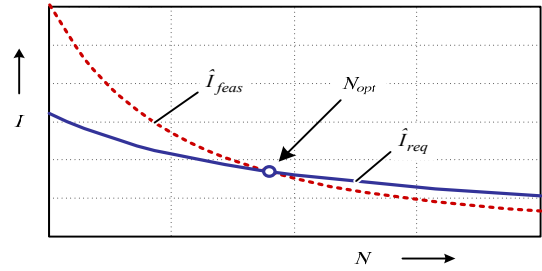

Fig. 11 General scaling properties of the required phase current $\hat{I}_{req}$ and the maximum feasible current $\hat{I}_{feas}$ in dependency on the winding number N

winding number N_{opt} will be at the intersection of $\hat{I}_{req}$ and $\hat{I}_{feas}$ and can be found by equalizing the currents in (12) and (14) for the case of separated coils:

$$N_{opt,s} = \frac{15 \, k_u \, U_{DC}}{n \cdot \sqrt{3600 \, k_u^4 + \pi^2 \, k_L^2 \, k_P^2 \, n^2}}. \tag{15}$$

For a higher number of turns the required power could not be delivered anymore (due to $\hat{I}_{feas} < \hat{I}_{req}$) and a lower number of turns would result in higher occurring currents (and therefore losses). Thus, N_{opt} is the optimal number of turns regarding losses for satisfying a specific power requirement P_{req}. A good pump design usually results in equivalent contributions of the two terms below the square root in (15) for medium rotation speeds. For high speeds the second term is dominant and the optimum winding number results in

$$N_{opt,s} = \frac{15 \, k_u \, U_{DC}}{\pi \, k_L \, k_P \, n^2} \quad \textit{for high speed} \tag{16}$$

while for low rotation speeds the optimum number is

$$N_{opt,s} = \frac{U_{DC}}{4\, k_u\, n} \quad \textit{for low speed.} \tag{17}$$

These approximations are important for a simplified subsequent analysis. In order to simplify the calculation of the resulting power electronics losses $P_{el,s}$ a square dependency of the semiconductor losses on the current is assumed. The total losses of all four full-bridges or eight half-bridges, respectively, can be written as

$$P_{el,s} = 4 \cdot k_{el} \cdot \underbrace{\left(\frac{\hat{I}_{req,s}}{\sqrt{2}} \right)^2}_{Drive} + 4 \cdot k_{el} \cdot \underbrace{\left(\frac{\hat{\Theta}_b}{\sqrt{2} \cdot N_{s,b}} \right)^2}_{Bearing} \tag{18}$$

Where k_{el} is a constant factor representing the sum of all loss constants per half-bridge and $N_{s,b}$ is the winding number of the bearing phase. In general, since no induced voltage is appearing in the bearing phase due to the specific winding arrangement (cf. section 2), the number of bearing windings $N_{s,b}$ can be chosen at a very high amount so that almost no current is needed to generate the required bearing ampere-turns Θ_b. In this case, the power electronics losses caused by the bearing can be neglected, which leads to a simplification of (18):

$$P_{el,s} = 2 \cdot k_{el} \cdot \hat{I}_{req,s}^2 \quad \text{for} \quad N_{s,b} \to \infty \tag{19}$$

Here, the appearing current $\hat{I}_{req,s}$ is given by evaluation of (12) for the optimum number of turns according to (16) and (17), respectively. In many practical cases high bearing ampere-turns with the drive frequency (e.q. for the case of a constant global force acting on the rotor in the case of centrifugal pumps) have to be impressed. Since the inductance value of the bearing coil is growing with N^2 and an increased inductance value is limiting the maximum feasible current for a specific electrical frequency ω_{el} also for the bearing a lower number of bearing windings can be required for satisfying dynamics. For the exemplarily case of the same number of windings for the bearing and drive coils (which represents a worst-case assumption), the power electronics losses can be written to

$$P_{el,s} = 2 \cdot k_{el} \cdot \hat{I}_{req,s}^2 \cdot \left(1 + \frac{\hat{\Theta}_b^2}{\hat{\Theta}_d^2} \right) \quad \text{for} \quad N_{s,b} = N_{opt,s}. \tag{20}$$

4.2 Combined Coils

For the winding configuration with combined coils, all coils with the inductance $L_c = k_L \cdot N_c^2$ and an induced voltage $\hat{U}_{ind,c} = k_u \cdot n \cdot N_c$ are lying in parallel (cf. Fig. 10(b)). It is important to mention that due to the same motor setup and iron circuit (cf. Fig. 1) the factors k_L and k_u are identical to the case of separated coils. For the same needed mechanical power delivered by four combined phases (which is equivalent to one drive phase in the case of separated coils) as depicted in Fig. 10(b) the current requirement per phase is given by

$$\hat{I}_{req,c} = \frac{k_P\, n}{2\, k_u\, N_c}. \tag{21}$$

Interestingly, this current is equal to $\hat{I}_{req,s}$ for the same number of windings $N_s = N_c$. However, (21) only defines the needed drive current per coil to build up the required torque. As mentioned before, in the case of combined coils an additionally superposed bearing current, given by the needed ampere-turns Θ_b, has to be impressed in the same coils. For the calculation of the optimum winding number $N_{opt,c}$ the maximum appearing worst-case current has to be taken into consideration. Looking at $\Theta_{c,5}$ in (5), for example, one can see that for the case of $\varphi = 0$ the bearing and drive currents are in phase and therefore the maximum worst-case current appears according to

$$\hat{I}_{req,c,worst-case} = \hat{I}_{req,c} \cdot \left(1 + \frac{\hat{\Theta}_b^2}{\hat{\Theta}_d^2} \right). \tag{22}$$

In contrast to the separate configuration, now the coils are star-connected, which means that only half the DC-link voltage $U_{DC}/2$ appears over each coil. With this, the maximum feasible current in case of combined coils is given by

$$\hat{I}_{feas,c} = \frac{60 \cdot \sqrt{\left(\frac{U_{DC}}{2} \right)^2 - k_u^2 \cdot n^2 \cdot N_c^2}}{2\, \pi\, n\, k_L\, N_c^2}. \tag{23}$$

The resulting optimum winding number for combined coils can be found in an analogous manner as for separated coils with the previously mentioned simplifications by equalizing (22) and (23) for high rotation speed

$$N_{opt,c} = \frac{15\,k_u\,U_{DC}}{\pi\,k_L\,k_P\,n^2} \cdot \frac{2\,\hat{\Theta}_d}{\hat{\Theta}_d + \hat{\Theta}_b} \qquad (24)$$

and for low rotation speed

$$N_{opt,c} = \frac{U_{DC}}{2\,k_u\,n}. \qquad (25)$$

Now, the total appearing power electronics losses for combined coils can be calculated by summing up the losses of all eight half-bridges:

$$P_{el,c} = k_{el} \cdot \sum_{i=1}^{8} \left(\frac{\Theta_{c,i,rms}}{N_{opt,c}} \right)^2. \qquad (26)$$

Solving (26) by inserting (5) and (1) leads to the total power electronics losses in case of combined coils in dependency on the needed drive current $\hat{I}_{req,c}$ per coil and the ampere-turns ratio:

$$P_{el,c} = 4 \cdot k_{el} \cdot \hat{I}_{req,c}^2 \left(1 + \frac{\hat{\Theta}_b^2}{\hat{\Theta}_d^2} \right). \qquad (27)$$
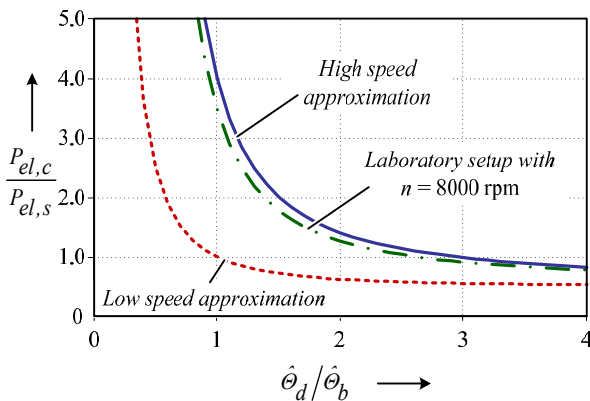

Fig. 12 Power electronics loss reduction by using combined coils in dependency on the ampere-turns ratio Θ_d/Θ_b

Inserting the required drive currents for separated and combined coils out of (12) and (21) into the equations for the power electronics losses (19) and (27) leads finally to the power electronics loss ratio for high rotation speeds[2]

$$\frac{P_{el,c}}{P_{el,s}} = \frac{\left(\hat{\Theta}_b + \hat{\Theta}_d\right)^2 \cdot \left(\hat{\Theta}_b^2 + \hat{\Theta}_d^2\right)}{2\,\hat{\Theta}_d^4} \qquad (28)$$

and with the approximation for low rotation speeds

$$\frac{P_{el,c}}{P_{el,s}} = \frac{\hat{\Theta}_b^2 + \hat{\Theta}_d^2}{2\,\hat{\Theta}_d^2}. \qquad (29)$$

These resulting power electronics loss ratios for low and high rotation speeds in dependency on the ampere-turns ratio are depicted in Fig. 12. One can see that for an ampere-turns ratio of 1 the power electronics losses for combined coils will be equal for low speeds and are four times higher for high speeds with respect to the separated coils. This means that for applications, where the pump power is relatively low (low to medium pressure pumps) and/or the bearing requirements are large, significantly higher losses appear in the power electronics inverter if the setup with combined windings is chosen. However, for typical values of the ampere-turns ratio Θ_d/Θ_b in the range of 2-3 and high targeted rotation speeds, the appearing power electronics losses are in a similar range. In Fig. 12 also a calculated curve by using (15) with experimentally derived constants k_L, k_P and k_u from the laboratory setup, as will be shown in section 6, for a rotation speed of 8000 rpm is depicted. The values for the constant factors have been found experimentally to $k_L = 1.2 \cdot 10^{-7}$ [H], $k_P = 1.3 \cdot 10^{-6}$ [Ws^2] and $k_u = 5.5 \cdot 10^{-6}$ [Vs]. This shows the validity of the high speed approximation according to (16) and (24).

Again, an interesting result is the independence of the power electronics loss ratio on the load angle φ, whereas the separate losses per half-bridge are still, analogous to the copper losses, dependent on the load angle φ.

---

[2] Only the case of an infinite number of bearing windings in case of separated coils was considered for sake of simplicity.

5. Maximum achievable pump pressure and speed

As mentioned in the introduction, the general demand for bearingless pump systems for high hydraulic pressure applications is rising. The need for an increased output pressure at a constant hydraulic flow rate leads to the required mechanical power and furthermore the phase currents given in (12) for separated and (21) for combined coils. Since the achievable output pressure is growing with n^2, the demand for high hydraulic output pressure translates to a maximization of the rotation speed. In this section, the maximum achievable rotation speeds for the setups with separated and combined coils will be calculated and compared.

5.1 Separated Coils

Combining the required current according to (12) with the optimum number of windings, given in (16) (approximation for high rotation speeds), leads to

$$\hat{I}_{req,s} = \frac{\pi \, k_L \, k_P^2 \, n^3}{30 \, k_u^2 \, U_{DC}}. \tag{30}$$

Equalizing (30) with the maximum allowed current per half-bridge I_{max} and solving by n leads to the maximum achievable rotation speed for separated coils:

$$n_{max,s} = \sqrt[3]{\frac{30 \, I_{max} \, k_u^2 \, \pi \, U_{DC}}{\pi \, k_L \, k_P^2}}. \tag{31}$$

5.2 Combined Coils

The maximum achievable speed for the setup with combined coils can be calculated in a similar manner as for separated coils. In this case the maximum appearing worst-case current according to (22) has to be taken into consideration for the calculation of $n_{max,c}$. By inserting the optimum winding number for the combined coils given in (24) (approximation for high rotation speeds), one obtains

$$\hat{I}_{req,c,worst-case} = \frac{\pi \, k_L \, k_P^2 \, n^3}{60 \, k_u^2 \, U_{DC}} \cdot \frac{\left(\hat{\Theta}_b + \hat{\Theta}_d\right)^2}{\hat{\Theta}_d^2}. \tag{32}$$
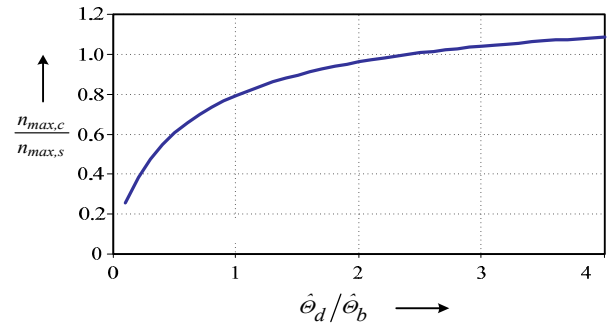

Fig. 13 Maximum achievable speed ratio over the ampere-turn ratio. Θ_d/Θ_b

Again, equalizing (32) with the maximum allowed current per half-bridge I_{max} and solving by n leads to the maximum achievable speed for combined coils in dependency on the ampere-turns ratio:

$$n_{max,c} = \sqrt[3]{\frac{60 \, I_{max} \, k_u^2 \, U_{DC} \, \hat{\Theta}_d^2}{\pi \, k_L \, k_P^2 \left(\hat{\Theta}_b + \hat{\Theta}_d\right)^2}}. \tag{33}$$

Finally, the maximum achievable speed ratio can be written in dependency on the ampere-turns ratio

$$\frac{n_{max,c}}{n_{max,s}} = \sqrt[3]{\frac{2 \, \hat{\Theta}_d^2}{\left(\hat{\Theta}_b + \hat{\Theta}_d\right)^2}} \tag{34}$$

and is depicted in Fig. 13. One can see that for high bearing requirements and/or low to medium drive requirements significantly higher rotation speeds can be achieved with separated coils. However, since for high pressure pump applications typical ampere-turns ratios are in the range between 2 and 3, the maximum achievable speed of both winding setups is comparable.

6. Experimental Verification

To verify the previously done examinations, laboratory setups for separated (Fig. 14(a)) and combined coils (Fig. 14(c)) have been built up. Both setups are driven by the same power electronics, which is shown in Fig. 14(b) with the only difference that the separated coils are energized by full-bridges (cf. Fig. 9(a)), whereas the combined coils
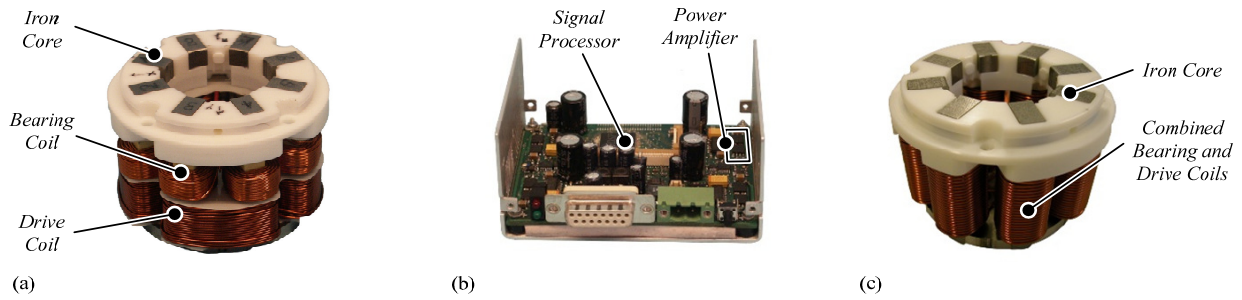
Fig. 14 (a) Experimental setup with separated coils with the drive coils wound over two claws and a resulting winding length factor $k_{lm} = 0.9$; (b) power electronics with eight half-bridge inverters; and (c) combined coils

are star-connected and energized by eight half-bridges (cf. Fig. 9(b)). Furthermore, for the control of the eight currents in the combined coils eight current sensors (instead of four) have been employed. In the following section measurements with both setups will be shown to prove the previous results. For both setups the DC-link voltage was chosen to 48 V with a maximum allowed peak current per half-bridge $I_{max} = 10$ A.

First, current measurements for both setups are shown in Fig. 15. For separated coils (Fig. 15(a)) the load angle φ, which depends on the specific orientation of the pump outlet, can be found between the drive $i_{d,1}$ and the bearing current $i_{b,1}$. Additionally, it can be seen that the bearing currents show lower values in comparison to the drive current which is a consequence of the higher number of windings $N_{s,b}$ for the bearing coils.

In the case of combined coils the phase currents are a superposition of the needed drive and bearing currents and are consequently characterized by different amplitudes and phase shifts as can be seen in Fig. 15(b) (phase currents $i_{c,1}$, $i_{c,2}$ and $i_{c,3}$).

For the verification of the copper loss reduction as
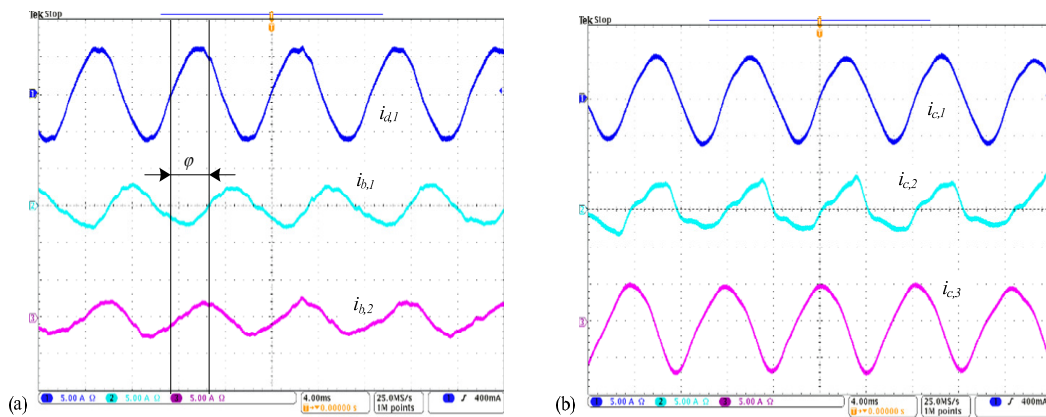

Fig. 15 Current measurements for separated and combined setups with the same hydraulic load of 14 l/min and 1.1 bar outlet pressure. Figure (a) shows one drive and both bearing currents in case of separated coils. Figure (b) on the right hand side shows the currents flowing in the coils 1, 2 and 3 in case of combined coils (current scale 5 A/div, time scale 4 ms/div)

shown in section 3 several measurements with different load and speed conditions have been done and are illustrated in Fig. 16 together with the predicted loss reduction curve for the case of $k_{lm} = 0.9$. Hereby, each point indicates the ratio of the experimental measured copper losses appearing in the two setups for the same operating point. One can see that the measurements show a significant copper loss reduction by using combined coils and the measured loss reduction basically fits with the estimated loss reduction. Furthermore, the power electronics losses have been measured and compared for these operation points. One can see that they basically fit with the predicted curve and that the ratio is between 1 and 2 (cf. Fig. 16). For the design at hand (160 W

Table 1 Measurements for the laboratory setups shown in Fig. 14 designed for $P_{mech} = 160$ W with the maximum achieved rotation speeds $n_{max,s} = 9500$ rpm and $n_{max,c} = 8000$ rpm

#	Θ_d/Θ_b	P_{mech} [W]	$P_{cu,s}$ [W]	$P_{cu,c}$ [W]	$P_{el,s}$ [W]	$P_{el,c}$ [W]
1	1.2	130	18.6	8.4	2.4	4.6
2	1.7	50	7.6	3.8	1.5	2.3
3	1.8	55	8.2	4.4	1.8	2.6
4	2.3	155	40.0	30.0	4.5	6.5
5	3.0	115	18.5	13.9	2.8	3.4

mechanical power) a maximum speed of 8000 rpm has been achieved with combined coils, whereas 9500 rpm has been achieved with separated coils. A compilation of the measured data is given in Table 1.

7. Conclusions

In this paper two different winding concepts for bearingless pumps have been discussed. The comparison was based on the assumptions of the same needed force and torque in both cases, same dimensions, same iron circuit, same magnet size and magnetization, same maximum current density and finally the same winding factor in the coils. The concepts have been compared concerning the copper losses, the power electronics losses and the maximum achievable rotation speed which
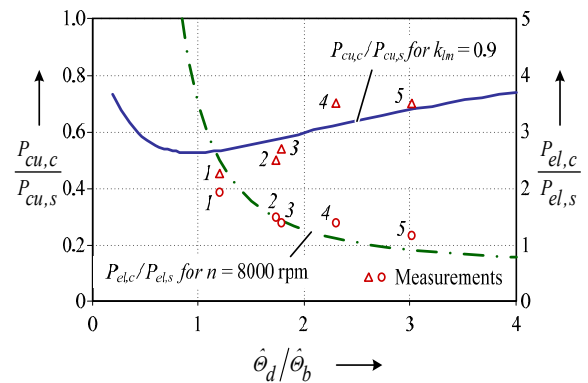

Fig. 16 Copper loss ratio $P_{cu,c}/P_{cu,s}$ and electronics loss ratio $P_{el,c}/P_{el,s}$ over ampere-turn ratio for an average winding length factor of $k_{lm} = 0.9$ (cf. Fig.7) with measurements done with the laboratory setups at several load and speed conditions (for pairwise equal hydraulic conditions): **1**: 7000 rpm, $P_{mech} = 130$ W; **2**: 7000 rpm, $P_{mech} = 50$ W; **3**: 6000 rpm, $P_{mech} = 55$ W; **4**: 8000 rpm, $P_{mech} = 155$ W; **5**: 7000 rpm, $P_{mech} = 115$ W

translates to a maximum pump pressure.

The most remarkable difference between the two concepts is the aspect of the copper losses, where a realistic reduction of about 30%-40% can be achieved by using combined coils. Regarding the coil volume, there is a trade-off situation between the coil volume and the copper losses, i.e. the copper loss reduction by combined coils can be alternatively used for a reduction of the coil volume.

The calculations for the copper and electronics loss comparison are based on the assumption of sinusoidal bearing and drive currents and a load angle φ, which is occurring between the bearing and the drive currents and is dependent on the orientation of the outlet of the centrifugal pump.

Basically, for the combined coils twice the numbers of phases have to be energized by the inverter. However, if the same power shall be delivered to the pump in order to perform a fair comparison, the combined coils can be driven by eight half-bridges with the same current and voltage ratings for the semiconductors and supplied by the same DC-link voltage. The examinations in this paper have shown that in the case of combined coils the power electronics losses are highly dependent on the needed

bearing ampere-turns and that significantly larger losses occur for low drive and/or high bearing requirements. However, for typical high pressure applications both setups are in a comparable range concerning the power electronic losses.

Regarding the maximum achievable speed, for low drive and/or high bearing requirements again the combined coils are clearly inferior. However, for high pressure applications the combined coils again show almost the same performance.

As to manufacturability, there is an apparent advantage for the combined coils, both in terms of number and uniformity. On the other hand, the control of the eight currents (instead of four) leads to a clearly higher effort for the combined coils, including a higher number of current sensors. Finally, also the cabling effort between the pump and the power electronics has to be taken into account, which is double for the combined coils.

Therefore, the decision regarding the preferable winding concept has to be taken on a case to case basis depending on the specific application, since both concepts have their advantages in different aspects. However, for given specifications, the calculations and considerations detailed in this paper can serve as a guideline for the selection of the appropriate winding concept.

References

[1] A. Chiba, T. Fukao, O. Ichikawa, M. Oshima, M. Takemoto, and D. G. Dorrell, Magnetic Bearings and Bearingless Drives. Elsevier, 2004.

[2] M. Neff, "Bearingless pump system for the semiconductor industry", in *6th International Symposium on Magnetic Suspension Technology*, pp. 169–173, 2001.

[3] R. Schoeb, "Centrifugal pump without bearings or seals", World Pumps, Vol. 430, pp. 34–37, 2002.

[4] T. Nussbaumer, K. Raggl, P. Boesch, and J.W.Kolar, "Trends in integration for magnetically levitated pump systems", in *PCC Nagoya*, pp. 1551–1558, 2–5 April 2007.

[5] M. Bartholet, S. Silber, T. Nussbaumer, and J. Kolar, "Performance investigation of two-, three- and four-phase bearingless slice motor configurations", in *Power Electronics and Drive Systems, 2007. PEDS '07. 7th International Conference on*, pp. 9–16, 27-30 Nov. 2007.

[6] K.-Y. Cho, "Sensorless Control for a PM Synchronous Motor in a Single Piston Rotary Compressor", *Journal of Power Electronics*, Vol. 6, No. 1, pp.29-37, 2006.

[7] Y. Yamamoto, H. Funato, and S. Ogasawara, "Hybrid Sensor–less Control of Permanent Magnet Synchronous Motor in Low–speed Region", *Journal of Power Electronics*, Vol. 8, pp. 301–308, 2008.

[8] S.-C. Yoon and J.-M. Kim, "Sensorless control of a pmsm at low speeds using high frequency voltage injection", *Journal of Power Electronics*, Vol. 5, pp. 11–19, 2005.

[9] T. Tera, Y. Yamauchi, A. Chiba, T. Fukao, and M. A. Rahman, "Performances of bearingless and sensorless induction motor drive based on mutual inductances and rotor displacements estimation", *IEEE Transactions on Industrial Electronics*, vol. 53, pp. 187–194, 2006.

[10] K. Raggl, T. Nussbaumer, and J. W. Kolar, "Comparison of Winding Concepts for Bearingless Pumps", in *ICPE*, 2007.

[11] M. Neff, "Bearingless centrifugal pump for highly pure chemicals", in *Proc. 8th ISMB*, pp. 283–287, Aug. 2002.

[12] R. Schoeb, "Principle and application of a bearingless slice motor", *JSME International Journal*, Vol. 40, No. 4, pp. 593–598, 1997.

[13] G. Schweitzer, "Active magnetic bearings — chances and limitations", *6th International Conference on Rotor Dynamics*, pp. 1–14, Oct. 2002.

[14] J. Bichsel, "The bearingless electrical machine", *International Symposium on Magnetic Suspension Technology*, Vol. 2, pp. 1–14, Aug. 19–23 1991.

[15] H. Zhu, Q. Cheng, Q. Wu, and W. Pan, "Radial Suspension Force Control of Bearingless Motor with Flux Equivalent Air–Gap Virtual Winding Current", in *11th International Symposium on Magnetic Bearings, ISMB11, Japan*, 2008.

[16] M. Oshima, S. Miyazawa, T. Deido, A. Chiba, F. Nakamura, and T. Fukao, "Characteristics of a permanent magnet type bearingless motor", in *Industry Applications Society Annual Meeting, 1994., Conference Record of the 1994 IEEE*, pp. 196–202 Vol.1, 2-6 Oct. 1994.

[17] M. Oshima, A. Chiba, T. Fukao, and M. Rahman, "Design and analysis of permanent magnet–type bearingless motors," *Industrial Electronics, IEEE Transactions on*, Vol. 43, No. 2, pp. 292–299, Apr 1996.

[18] B. Singh and S. Singh, "State–of–Art on Permanent Magnet Brushless DC Motor Drives," *Journal of Power Electronics*, Vol. 9, pp. 1–17, 2009.

[19] H. Wang, D.-H. Lee, and J.-W. Ahn, "Calculation of Suspending Force for New Bearingless Switched Reluctance Motor", in *11th International Symposium on Magnetic Bearings, ISMB11, Japan*, 2008.

[20] A. Chiba, R. Furuichi, Y. Aikawa, K. Shimada, Y. Takamoto, and T. Fukao, "Stable operation of induction-type bearingless motors under loaded conditions",

Industry Applications, IEEE Transactions on, Vol. 33, No. 4, pp. 919–924, Jul/Aug 1997.

[21] A. Chiba, D. Akamatsu, T. Fukao, and M. Azizur Rahman, "An improved rotor resistance identification method for magnetic field regulation in bearingless induction motor drives", *Industrial Electronics, IEEE Transactions on*, Vol. 55, No. 2, pp. 852–860, Feb. 2008.

[22] S. Silber, W. Amrhein, P. Bösch, R. Schöb, and N. Barletta, "Design aspects of bearingless slice motors", *IEEE/ASME Transactions on Mechatronics*, Vol. 10, No. 6, pp. 611–617, 2005.

[23] W. Amrhein, S. Silber, and K. Nenninger, "Levitation forces in bearingless permanent magnet motors", *IEEE Transactions on Magnetics*, Vol. 35, No. 5, pp. 4052–4054, 1999.

[24] Y. Okada, K. Dejima, and T. Ohishi, "Analysis and comparison of pm synchronous motor and induction motor type magnetic bearings", *Industry Applications, IEEE Transactions on*, Vol. 31, No. 5, pp. 1047–1053, Sep/Oct. 1995.

[25] Y. Okada, S. Miyamoto, and T. Ohishi, "Levitation and torque control of internal permanent magnet type bearingless motor", *Control Systems Technology, IEEE Transactions on*, Vol. 4, No. 5, pp. 565–571, Sep. 1996.

[26] W. K. S. Khoo, R. L. Fittro, and S. D. Garvey, "AC polyphase self–bearing motors with a bridge configured winding," in *Proc. 8th Int. Symp. Magnetic Bearings, Mito, Japan*, pp. 47–52, Aug. 2002.

[27] W. K. S. Khoo, "Bridge Configured Winding for Polyphase Self–Bearing Machines", *IEEE Transactions on Magnetics*, Vol. 41, No. 4, pp. 1289–1295, April 2005.

[28] J. A. D. Paiva, A. O. S. A. L. Maitelli, and R. M. Stephan, "Performance Improvement of a Split Winding Bearingless Induction Machine Based on A Neural Network Flux Observer", in *11th International Symposium on Magnetic Bearings, ISMB11, Japan*, 2008.

[29] K. Kuepfmueller, *Einfuehrung in die theoretische Elektrotechnik*. Springer Verlag Berlin, Vol. 11. Auflage, 1984.

Klaus Raggl was born in Zams, Austria, in 1980. He received the M.S. in Mechatronics from the Johannes Kepler University Linz, Linz, Austria, in 2005. Since 2005, he has been a Ph.D. student at the Power Electronics Systems Laboratory, ETH Zurich, Zurich, Switzerland, section drive technology and magnetic bearings, where he is currently working on bearingless pump systems with maximum power density.

Thomas Nussbaumer was born in Vienna, Austria, in 1975 and studied electrical engineering at the University of Technology Vienna, Austria, where he received his M.Sc. degree with honors in 2001. During his Ph.D. studies at the Power Electronic Systems Laboratory (PES) in the Swiss Federal Institute of Technology (ETH) Zurich, Switzerland, he performed research on the design, control and modulation of three--phase rectifiers with low effects on the mains. After receiving his Ph.D. degree in 2004, he has been continuing research on power factor correction techniques, modeling and dynamic control of three--phase rectifiers and electromagnetic compatibility at the PES/ETH. Since Feb, 2006 he has been with Levitronix GmbH, where he is currently working on magnetically levitated motors and pumps for the semiconductor process industry.

Johann W. Kolar (M'89–SM'04) received his Ph.D. degree (summa cum laude / promotio sub auspiciis praesidentis rei publicae) from the University of Technology Vienna, Austria. Since 1984 he has been working as an independent international consultant in close collaboration with the University of Technology Vienna, in the fields of power electronics, industrial electronics and high performance drives. He has proposed numerous novel PWM converter topologies, and modulation and control concepts, e.g., the VIENNA Rectifier and the Three-Phase AC-AC Sparse Matrix Converter. Dr. Kolar has published over 250 scientific papers in international journals and conference proceedings and has filed more than 70 patents. He was appointed Professor and Head of the Power Electronic Systems Laboratory at the Swiss Federal Institute of Technology (ETH) Zurich on Feb. 1, 2001. The focus of his current research is on AC-AC and AC-DC converter topologies with low effects on the mains, e.g. for power supply of telecommunication systems, More-Electric-Aircraft and distributed power systems in connection with fuel cells. Further main areas are the realization of ultra-compact intelligent converter modules employing the latest power semiconductor technology (SiC), novel concepts for cooling and EMI filtering, multi-domain/multi-scale modeling and simulation, pulsed power, bearingless motors, and Power MEMS. He received the Best Transactions Paper Award of the IEEE Industrial Electronics Society in 2005. He also received an Erskine Fellowship from the University of Canterbury, New Zealand, in 2003. In 2006, the European Power Supplies Manufacturers Association (EPSMA) awarded the Power Electronics Systems Laboratory of ETH

Zurich as the leading academic research institution in Europe. Dr. Kolar is a Member of the IEEE and a Member of the IEEJ and of Technical Program Committees of numerous international conferences in the field (e.g. Director of the Power Quality Branch of the International Conference on Power Conversion and Intelligent Motion). From 1997 through 2000 he has been serving as an Associate Editor of the IEEE Transactions on Industrial Electronics and since 2001 as an Associate Editor of the IEEE Transactions on Power Electronics. Since 2002 he also is an Associate Editor of the Journal of Power Electronics of the Korean Institute of Power Electronics and a member of the Editorial Advisory Board of the IEEJ Transactions on Electrical and Electronic Engineering.